UNIABUJA Journal of Engineering and Technology

https://ujet.uniabuja.edu.ng/
Special Issue

Numerical Analysis of The Combustion Process Design Parameters of A Locally Made Cook Stove Burner

Olalekan O. OLAMIDE[1,*], Emmanuel O. AYOOLA[1], Kehinde L. OLAITAN[1], Mufutau A. WAHEED[1]

[1]*Department of Mechanical Engineering, Federal University of Agriculture, Abeokuta*

[1*]*olamideoo@funaab.edu.ng*, [2]*ayoolatosindee@gmail.com*, [3]*olaitankl@funaab.edu.ng*, [4]*waheedma@funaab.edu.ng*

Abstract
The design and continuous improvement of clean, efficient and locally made cookstove burners are critical for reducing emissions and improving energy access in Nigeria. This study presents a numerical analysis of propane combustion in a locally made commercial cookstove burner using ANSYS Fluent 2022 R1. A two-dimensional model based on a co-flow, non-premixed air/fuel configuration was used to solve the governing equations of continuity, momentum, energy and species transport, and to simulate the flame structure, temperature distribution and species concentrations. Combustion kinetics were represented with a two-step global reaction mechanism, and CO_2, CO, soot and NO_x formation were computed alongside combustion efficiency. The fuel port diameter was varied from 1 to 5 mm and the fuel pressure from 1500 to 3000 Pa, comparable to regulated pressures in practical burners, while the air velocity ranged from 1.5 to 3.5 m/s at atmospheric pressure. The model was validated against experimental data from the literature, with velocity and temperature differing by less than 5%. A port diameter of 1 mm and an air inlet velocity of 2.5 m/s gave the highest flame temperature of about 2010 K. Propane was almost fully consumed within the domain, while the maximum mole fractions of CO_2, CO and soot were about 0.07, 0.132 and 0.0076 respectively. NO_x formation followed peak flame temperature, and the highest combustion efficiency of 45.50% occurred at 2500 Pa. The results show that locally made cookstoves can compete with imported ones when design parameters are optimised for better efficiency and lower emissions.

Keywords: *Simulation, propane, combustion, emission, cookstove.*

1.0 Introduction

Cookstoves play a role in the lives of approximately 3.5 billion people globally, particularly in low-income countries like Nigeria and India, where they serve essential functions like cooking meals and heating homes (Rosenthal et al., 2018). There are still about 2.1 billion people who cook using open fires or inefficient stoves fuelled by biomass like charcoal, wood, animal dung, and agricultural residues, which causes significant air pollution. An estimation of 3.2 million deaths was recorded throughout the year 2020, including more than 237,000 deaths of children under the age of five, attributed to household air pollution. Every year, 6.7 million premature deaths are linked to the combined impacts of household outdoor air pollution (Bozzola et al., 2024). Exposure to household air pollution is known to cause lung cancer, chronic obstructive pulmonary disease (COPD), ischaemic heart disease, and stroke, among other non-communicable diseases.

The transition to cleaner fuels like liquified petroleum gas (LPG) is often hindered by high upfront costs for appliances, inconsistent supply chains, and the unaffordability of the fuel itself (Puzzolo et al., 2019). Modern cookstoves have the potential to reduce harmful emissions associated with traditional cooking methods. The burner plays a major role in the cookstove design by ensuring fuel burns cleanly and efficiently through factors such as air-fuel mixing and port size. Studies on locally made burners in Nigeria are scarce. However, Fakinle et al. (2019) conducted a comprehensive laboratory study of the thermal efficiency and emissions of conventional LPG burners widely used in Nigeria. The results revealed that most burners achieved average thermal efficiencies of 66.3% ± 7.2%. However, CO emissions exceeded safety thresholds in some cases.

Computational fluid dynamics (CFD) based models are useful in the simulation of combustion by predicting temperature distributions and emission rates, which may be used to improve stove designs. Husain et al. (2019) utilised a computational fluid dynamics model to optimise the geometry of a biomass cookstove to accomplish uniform air–fuel dispersion. Setiawan et al. (2018) carried out a CFD simulation to predict the temperature distribution and flow pattern in a biomass cooking stove. Sowgath et al. (2015) used a CFD model

Received: 27-05-2026 / Accepted: 11-06-2026 / Published: 22-08-2026

https://doi.org/10.70118/ujet.2026.sp01.15

to improve the emission characteristics and energy efficiency of a cookstove. Ali et al. (2017) investigated heat transfer emission characteristics of a cookstove using a CFD model. These studies show that CFD is a useful tool for studying different characteristics of a cookstove during combustion because it provides a cost-effective, accurate tool for improving cookstove design by allowing engineers to visualise complex phenomena like velocity fields, turbulent eddies, temperature gradients, and chemical species distribution. By simulating reacting flows inside the burner combustion chamber, engineers can analyse how changes in geometry affect flame stability, combustion efficiency, and emissions.

The objective of this study is to perform the numerical analysis of a section of a locally produced LPG burner to predict temperature distributions, combustion efficiency, and emissions through the use of CFD.

2.0 Methodology

The numerical analysis of LPG combustion in the cookstove burner was simulated using the finite volume method (FVM), which solves the governing equations of continuity, momentum, energy, and species transport using the CFD software, ANSYS Fluent 2022 R1.

Geometry and Mesh

The geometry of the locally made LPG cookstove burner with the dimensions in inches is shown in Figure 1. The computational domain modelled the physical burner as a simplified 2-dimensional cross-section of the multiple-port cookstove LPG burner, which was created using ANSYS Space Claim 2022. The computational domain encompasses the fuel supply, three burner ports, and the open combustion space above the burner. Figure 2 provides a view of the computational domain in ANSYS Fluent. Propane flows in through the fuel inlet under regulated pressure into the combustion zone, which represents the environment that is just above the burner, and moves in a co-flow configuration with air. Combustion takes place in this zone; the products exit the domain through the outlet.

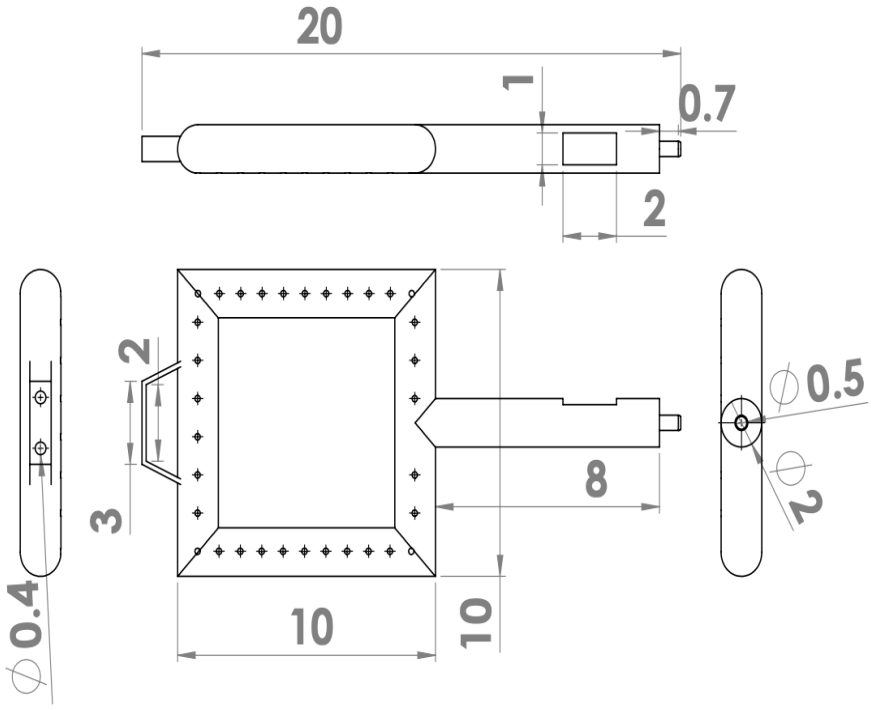

Figure 1: Engineering drawing of complete burner component

https://doi.org/10.70118/ujet.2026.sp01.15

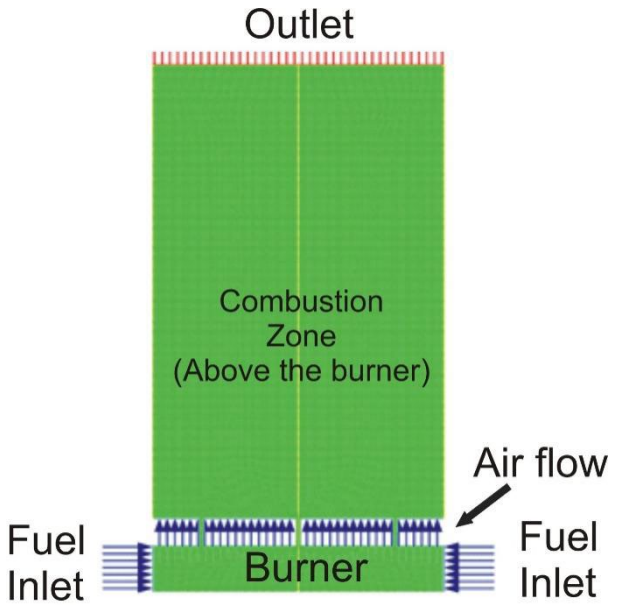

Figure 2: Computational Domain in ANSYS Fluent 2022 R1

The burner ports were configured as circular orifices; their diameters varied as a primary design parameter. The burner head aids in the distribution of the fuel to these ports. The overall dimensions of the combustion chamber were set up to properly capture the full flame development and its interaction with the surrounding air in the environment.

To reduce computation cost resources, the domain was divided into two as shown in Figure 3. The line of symmetry mirrors the other half of the domain. A computational mesh (Figure 4) consisting of 12382 elements and 12734 nodes was generated to discretise the fluid domain using ANSYS Meshing. The final mesh density was not adopted from the software default; it was established through a grid-independence study in which the element count was progressively refined until the predicted peak flame temperature and outlet species mole fractions changed by less than 1% between successive levels. A finer resolution was imposed in the regions of steep gradients, namely the burner ports and the reaction zone, while a coarser mesh was retained in the far field to limit the computational cost. The mesh quality was assessed using the standard skewness and orthogonal-quality metrics recommended for ANSYS Fluent, with the maximum skewness kept below 0.85 to ensure solution stability and convergence.

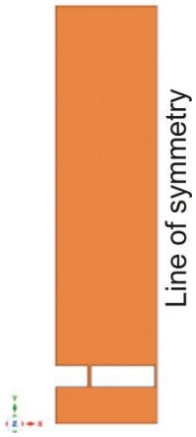

Figure 3: The geometry of the computational domain in ANSYS Space Claim

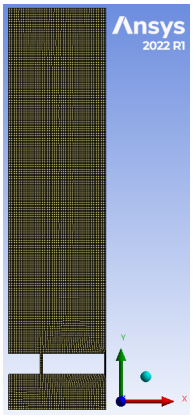

Figure 4: Meshing of the computational domain

Governing Equations and Physical Models

The various equations used to model the flow, heat transfer, and combustion simulation are presented in this section.

Propane Combustion

A two-step global reaction mechanism (propane-air-2 step) was employed to model the chemical kinetics of propane combustion. This simplified mechanism was selected to balance computational efficiency with the

https://doi.org/10.70118/ujet.2026.sp01.15

capability to accurately represent overall heat release, the formation of major products (CO2, H2O), and an important intermediate (CO). The two global reactions typically represented are:

$C_3H_8 + 3.5\ O_2 \rightarrow 3CO + 4H_2O$ (1)

$CO + 0.5O_2 \rightarrow CO_2$ (2)

The Eddy-Dissipation Model (EDM) of Magnussen and Hjertager (1977) was utilised to account for the interaction between turbulence and chemical reactions. The model assumes that the reaction rates in turbulent flows are controlled by the rate of turbulent mixing of the reacting eddies, characterised by the turbulent mixing time scale k/ε, rather than by the detailed Arrhenius kinetics. For a reaction r, the net rate of production of species i, $R_{i,r}$, is taken as the smaller of the two limiting rates governed by the reactant and product mass fractions, as given in Eqns. (3) and (4).

$$R_{i,r} = \nu'_{i,r} M_{w,i} A \rho \frac{\varepsilon}{k} \min_R \frac{Y_R}{\nu'_{R,r} M_{w,R}} \quad (3)$$

$$R_{i,r} = \nu'_{i,r} M_{w,i} A B \rho \frac{\varepsilon}{k} \frac{\sum_P Y_P}{\sum_j \nu''_{j,r} M_{w,j}} \quad (4)$$

where $R_{i,r}$ is the net rate of production of species i in reaction r, $\nu'_{i,r}$ and $\nu''_{i,r}$ are the stoichiometric coefficients of species i as a reactant and as a product in reaction r, $M_{v,i}$ is the molecular weight of species i, Y_r is the mass fraction of any reactant R, Y^P is the mass fraction of any product P, ε/k characterises the turbulent mixing rate, and A and B are empirical constants taken as 4.0 and 0.5, respectively (Magnussen and Hjertager, 1977).

Conservation of mass

The continuity equation is given in Eq. (5).

$$\nabla \cdot (\rho \bar{v}) = 0 \quad (5)$$

where ρ represents the density of the fluid, $\bar{v}$ represents the velocity of the fluid. It is the velocity vector, which has both a magnitude and a direction.

Conservation of momentum

The momentum equation is given in Eq. (6).

$$\rho \frac{\partial \bar{v}}{\partial t} + \nabla \cdot (\rho \bar{v} \bar{v}) = \nabla \cdot (p + \tau) \quad (6)$$

where ρ represents the density of the fluid, $\bar{v}$ represents the velocity of the fluid, $\frac{\partial \bar{v}}{\partial t}$ is the transient term representing the change of velocity with time, p represents pressure, τ is the viscous shear stress.

The flow turbulent scales within the domain were modelled using the k-ε model. The k-ε equations of this model are defined by Eqns. (7) - (8) respectively.

$$\frac{\partial}{\partial t}(\rho k) + \frac{\partial}{\partial x_i}(\rho k u_i) = \frac{\partial}{\partial x_j}\left[\left(\mu + \frac{\mu}{\sigma_k}\right)\frac{\partial k}{\partial x_j}\right] + G_k + G_b - \rho\varepsilon - Y_M + Y_k \quad (7)$$

$$\frac{\partial}{\partial t}(\rho\varepsilon) + \frac{\partial}{\partial x_i}(\rho\varepsilon u_i) = \frac{\partial}{\partial x_j}\left[\left(\mu + \frac{\mu_t}{\sigma_\varepsilon}\right)\frac{\partial k}{\partial x_j}\right] + C_{1\varepsilon}\frac{\varepsilon}{k}(G_k + C_{2\varepsilon}G_b) - C_{2\varepsilon}\frac{\varepsilon^2}{k} + S\varepsilon \quad (8)$$

where G_k represents the production of turbulent kinetic energy caused by mean velocity gradients, while G_b accounts for the contribution from buoyancy effects. The turbulent viscosity, μ_t, is given by the expression:

$\mu_t = \rho\ C\mu\ k^2 / \varepsilon$

In this relation, C1ε, C2ε, Cμ, and σε are model constants with the following values: C1ε = 1.44, C2ε = 1.92, Cμ = 0.09, and σε = 1.3.

Conservation of Energy

The energy equation is given in Eq. (9).

$$\rho \frac{Dh}{Dt} = \frac{DP}{Dt} + \nabla \cdot (k \nabla \cdot T) + \mu\Phi + \dot{Q} \quad (9)$$

where $\frac{Dh}{Dt}$ is the rate of change of the fluid's specific enthalpy, $\frac{DP}{Dt}$ represents the rate of change of the fluid's pressure, $k\nabla \cdot T$ is the heat flux due to conduction, according to Fourier's Law, μ is the dynamic viscosity of the fluid, and Φ is the viscous dissipation function. $\dot{Q}$ is the rate of heat release.

Species Transport Equations

The species transport equation is given in Eq. (10) (Turns et al., 2000).

$$\frac{\partial(\rho Y_i)}{\partial t} + \nabla \cdot (\rho \bar{v} Y_i) = \nabla \cdot (\rho D_i \nabla Y_i) + R_i \quad (10)$$

Where Y_i is the mass fraction of species i, D_i is the diffusion coefficient of species i, R_i is the net rate of production of species i due to chemical reactions.

https://doi.org/10.70118/ujet.2026.sp01.15

Boundary Conditions

The following boundary conditions, which were imposed in the computational domain, are presented in Table 1.

Table 1: Boundary condition at air inlet

Boundary	Type	Velocity Magnitude	Temperature	Species mole fraction	Turbulence Specification
Air Inlet	Velocity Inlet	Varied from 1.5 m/s to 3.5 m/s during parametric studies	300 K	O_2 = 0.21, N_2 = 0.79	Turbulence Intensity (0.1%), Viscosity Ratio (1)
Fuel Inlet	Pressure Inlet	Varied from 500 Pa to 3000 Pa	300 K	Propane (C_3H_8) with a mole fraction of 1.0	Turbulence Intensity (1%), Hydraulic Diameter (0.086 m)
Outlet	Pressure Inlet	101325 Pa (Atmospheric)		1	Backflow Turbulence Intensity (1%), Backflow Hydraulic Diameter (0.36 m)

Parametric Study Design

A parametric study was conducted to evaluate the influence of key design operating parameters. The study progressed in three main stages:

The air inlet velocity was initially varied at 1.5, 2.5, and 3 m/s for different burner port diameters (1 mm, 2 mm, 3 mm, 4 mm, and 5 mm) while maintaining a constant fuel inlet pressure of 2750 Pa.

The air inlet velocity was varied at 1.5, 2.0, 2.5, 3.0, and 3.5 m/s, keeping the fuel inlet pressure constant at 2750 Pa.

The fuel inlet pressure was then varied from 500 Pa to 3000 Pa in steps of 500 Pa.

Combustion Efficiency

The combustion efficiency (ηcomb) of the burner was determined using the ratio of carbon dioxide to the sum of carbon dioxide and carbon monoxide (CO), as defined by Eqn. (11) (Diti and Šulc, 2024).

$$\eta_{comb} = \frac{CO_2}{CO_2+CO} \times 100 \quad (11)$$

3.0 Results and Discussion

Validation of the Numerical Model

The ANSYS Fluent model was validated by replicating the turbulent propane jet flame case of Schefer (2001). The axial profiles of propane mass fraction and axial velocity obtained from the present simulation were compared with the measured data, as shown in Figures 5 and 6, respectively. The simulated propane mass fraction decayed along the axis at the same rate as the reported data, confirming that the rate of fuel consumption and the mixing behaviour were correctly captured, while the axial velocity profile reproduced the characteristic jet decay observed in the case. The maximum deviation between the simulated and reported values was less than 5% for both the axial velocity and the temperature, which indicates good agreement between the present model and the experimental data in the literature. The maximum temperature of 2475.1 K predicted by the model also falls within the range of 2470 to 2480 K reported for an adiabatic air–propane flame by Hamzah (2015). The close agreement in both the species decay and the velocity field gives confidence that the adopted turbulence–chemistry interaction, mesh resolution and boundary conditions are adequate for the parametric simulations that follow.

https://doi.org/10.70118/ujet.2026.sp01.15

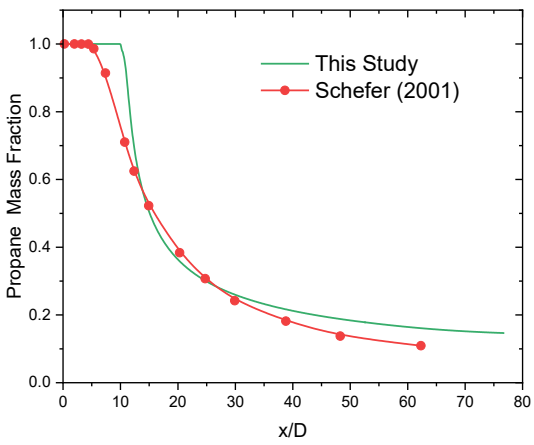

Figure 5: Validation graph of propane mass fraction against axial length based on the case of Schefer (2001)

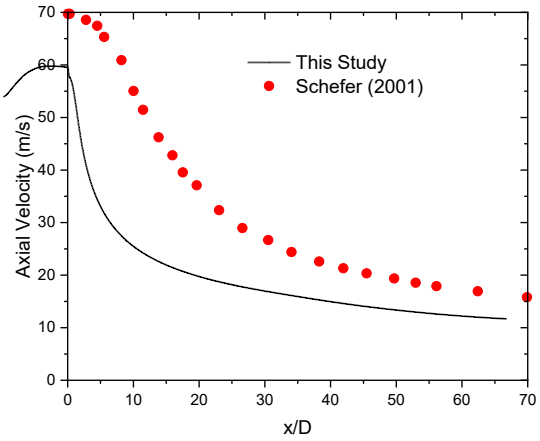

Figure 6: Validation graph of propane axial velocity against axial length based on the case of Schefer (2001)

Flow Characteristics and Mixing Patterns

The flow characteristics within the cookstove burner were analysed, focusing on the interaction between the incoming air, fuel jets, and the formation of combustion products. The distribution of propane and oxygen is shown in Figures 7 and 8, respectively. Propane concentrations were highest near the fuel inlet and decreased rapidly within the flame region as it was consumed. Oxygen concentrations were highest in the entrained air depleted significantly within the reaction zones, indicating their consumption during combustion. The regions where propane and oxygen concentrations overlapped rapidly diminished corresponded directly to the high-temperature flame zones, which reflect effective mixing and reaction.

The mixing patterns were highly dependent on the burner port diameter and the air inlet velocity. A smaller port diameter (1 mm) caused higher jet velocities at a specific fuel pressure. This improved mixing with the surrounding air, resulting in a more compact, intense flame. In contrast, larger port diameters produced lower jet velocities, possibly reducing mixing efficiency, leading to wider flame structures. The air inlet velocity played a critical role in controlling the overall air-to-fuel ratio and the rate of mixing. An optimal air velocity ensured sufficient oxygen supply without excessively quenching the flame.

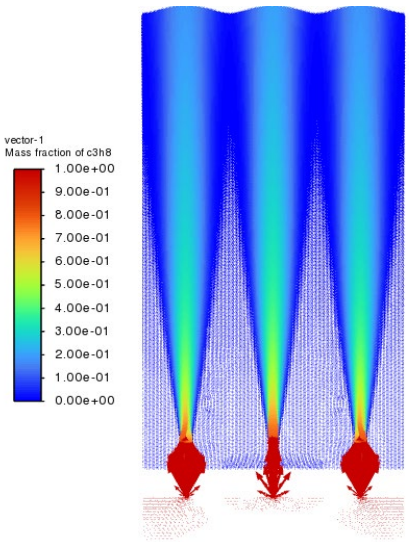

Figure 7: Representative Propane (C3H8) mass fraction contour of 1 mm port diameter at 2.5 m/s Air Inlet Velocity at 2500 Pa Fuel Inlet Pressure

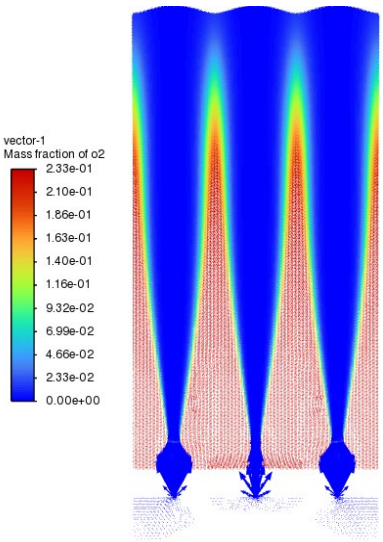

Figure 8: Representative Oxygen (O2) mass fraction contour of 1 mm port diameter at 2.5 m/s Air Inlet Velocity at 2500 Pa Fuel Inlet Pressure

https://doi.org/10.70118/ujet.2026.sp01.15

Temperature Distribution and Heat Transfer

The temperature distribution within the burner was a primary focus, as it directly impacts reaction rates and overall performance.

Effect of Port Diameter on Temperature

Figure 9 shows the peak temperatures in the domain as the burner port diameter is increased at a constant 2.5m/s air inlet velocity, and a constant 2750 Pa fuel inlet pressure.

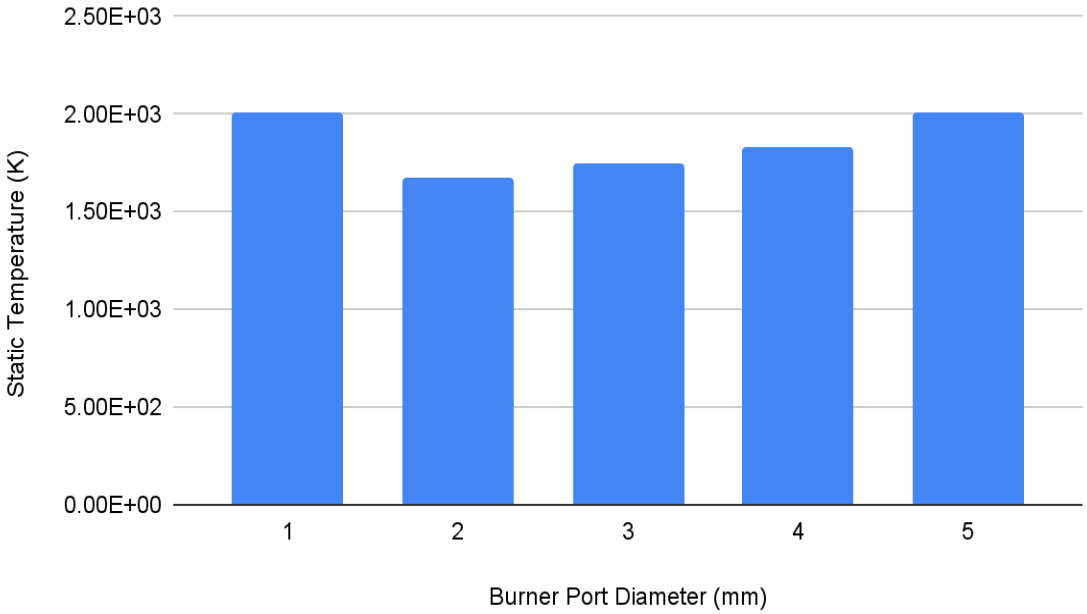

Figure 9: Pattern of peak temperature as the burner port diameter is increased at a constant 2.5m/s air inlet velocity, and a constant 2750 Pa fuel inlet pressure.

Initial investigations involved varying the burner port diameter (1 mm, 2 mm, 3 mm, 4 mm, 5 mm) at a constant fuel inlet pressure of 2750 Pa, for air inlet velocities of 2.5 m/s and 3 m/s. The temperature reduced briefly as the burner port diameter was increased, then increased through the next series of increments. Figures 10 and 11 show the temperature distributions for some of these cases. It was observed that the 1 mm port diameter yielded the highest peak flame temperatures across these conditions. This is attributed to the increased momentum of the fuel-air mixture exiting the smaller orifice, which promotes more efficient mixing and a more concentrated reaction zone. At an air inlet velocity of 2.5 m/s, the 1 mm port achieved a peak temperature of 2010 K. This result strongly supports a primary theme from the literature review in which burner geometry airflow dynamics are paramount to cookstove performance. These findings align with studies like Shahi et al. (2021), who showed that changing the burner circular geometry to a nozzle shape, reducing the nozzle angle, increased peak temperatures and thermal efficiency.

Effect of Air Velocity

The effect of varying air velocity was also studied, the 1mm burner port diameter was fixed, the air inlet velocity was further varied (1.5 m/s, 2.0 m/s, 2.5 m/s, 3.0 m/s, 3.5 m/s) at a constant fuel inlet pressure of 2750 Pa. Figures 12 - 13 presents the temperature contours for air velocity of 1.5 and 3 m/s, respectively for the port size of 1 mm while the maximum temperatures for various cases are shown in Table 2 and 3. The results confirmed that the 2.5 m/s air inlet velocity, combined with the 1 mm burner port diameter, produced the highest peak flame temperature of 2010 K. This optimal air velocity indicates a stoichiometric balance, where sufficient oxygen is supplied for complete combustion without quenching the flame. The peak temperature of 2010 K achieved in the present study is comparable to, and even exceeds, the temperatures reported in other numerical investigations. Dwivedi et al. (2020) achieved a maximum temperature of 1910 K by adding a flame shield to a burner, while Rimar et al. (2022) reported flame temperatures between 1600 K and 1750 K in their burner analysis.

https://doi.org/10.70118/ujet.2026.sp01.15

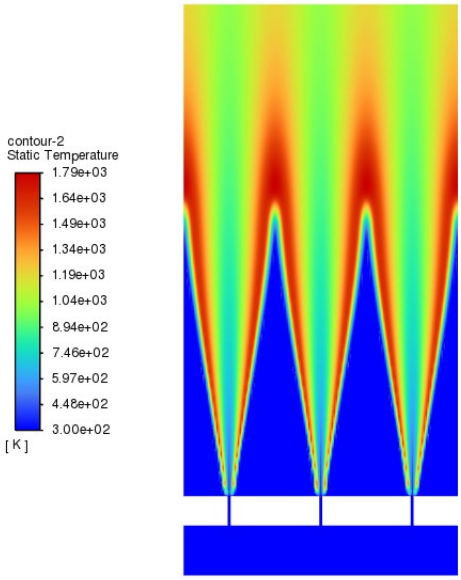

Figure 10: Temperature contour for 3 mm port diameter at 2.5 m/s

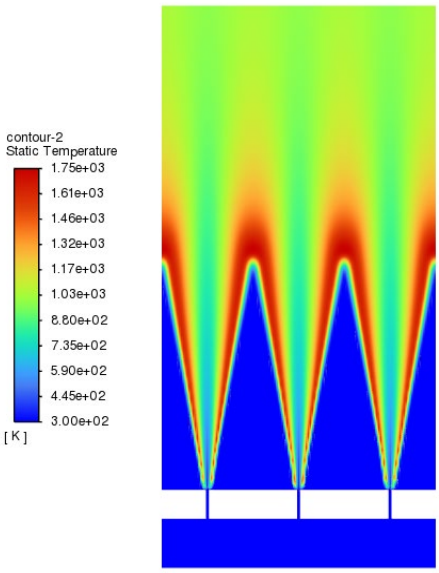

Figure 11: Temperature contour for 3 mm port diameter at 3 m/s

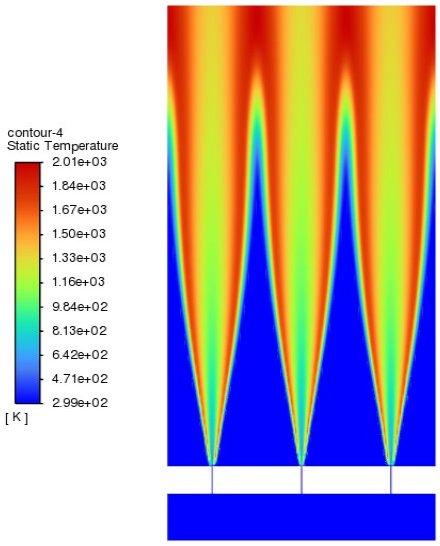

Figure 12: Temperature contour of 1 mm port diameter at 2.5 m/s

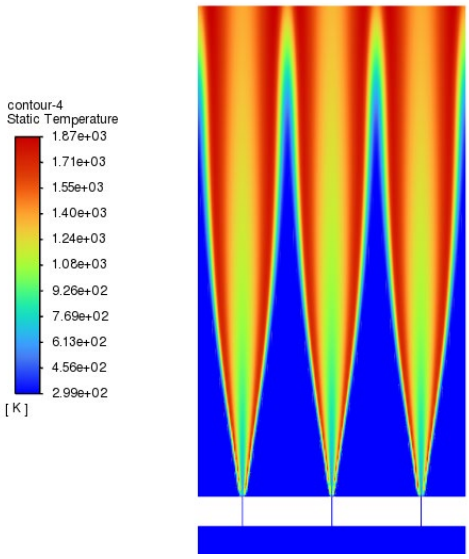

Figure 13: Temperature contour of 1 mm port diameter at 3 m/s

Table 2: Maximum temperature at varying burner port diameter with fuel pressure of 2750 Pa

Port Diameter (mm)	Air Inlet Velocity (m/s)	Temperature (K)
1	2.5	2010
1	3	1870
2	2.5	1830
2	3	1870
3	2.5	1750
3	3	1790
4	2.5	1670
4	3	1750
5	2.5	1650
5	3	1680

https://doi.org/10.70118/ujet.2026.sp01.15

Table 3: Static flame temperature at varying air inlet velocity magnitude with fuel pressure of 2750 Pa, with a port diameter of 1 mm

Burner Port Diameter (mm)	Air Inlet Velocity (m/s)	Temperature (K)
1	1.5	1920
1	2.0	1950
1	2.5	2010
1	3.0	1870
1	3.5	1850

Effect of Varying Fuel Inlet Pressure

The final set of simulations focused on varying the fuel inlet pressure (500 Pa, 1000 Pa, 1500 Pa, 2000 Pa, 2500 Pa, 3000 Pa) for the 1 mm burner port diameter, 2.5 m/s air inlet velocity. The graph of maximum flame temperatures observed for all cases considered is shown in Figure 14. The highest peak flame temperature of 2010 K was achieved at a fuel inlet pressure of 2500 Pa. This indicates that increasing the fuel flow rate up to this point, while maintaining optimal air supply, leads to a more intense reaction zone.

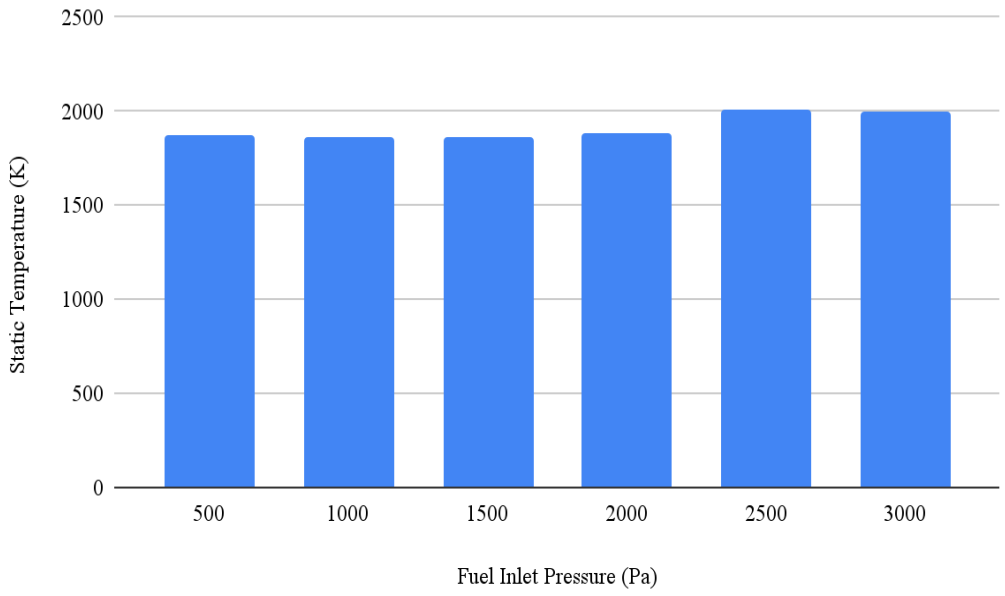

Figure 14: Pattern of peak temperature as the fuel inlet pressure is increased at a constant 2.5m/s air inlet velocity for a 1 mm burner port diameter.

The static temperature is briefly reduced and then increased as the next series of increments in fuel inlet pressure is analysed. 1 mm burner port diameter, 2.5 m/s air inlet velocity, and 2500 Pa fuel inlet pressure yielded the highest temperature during simulation. The temperature distribution contours for fuel inlet pressure of 500 to 2,500 Pa at an air velocity of 2.5 m/s are presented in Figures 15 and 16, respectively.

https://doi.org/10.70118/ujet.2026.sp01.15

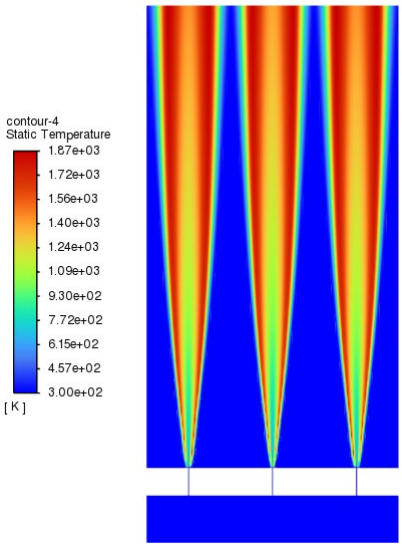

Figure 15: Temperature distribution for 1 mm port diameter at 500 Pa and 2.5 m/s air velocity

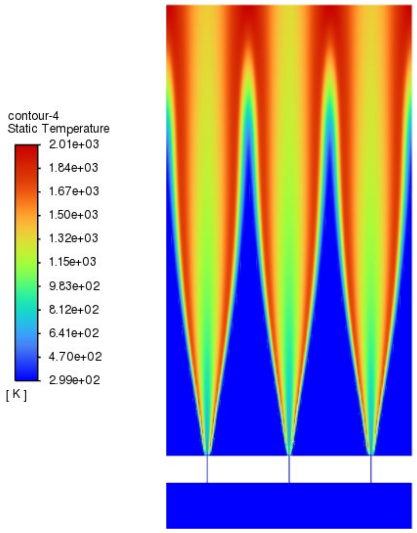

Figure 16: Temperature distribution for 1 mm port diameter at 2500 Pa and 2.5 m/s air velocity

Species Concentration of Combustion Products

The distributions of CO_2, CO, and unburnt C_3H_8, along with the formation of soot and NO_x, were examined for all cases, with particular attention to the fuel inlet pressure variations for the burner port diameter of 1mm and air velocity of 2.5 m/s.

CO_2 *and CO distributions*

Figure 17 shows the graph of CO2 emissions at various fuel pressures when the air velocity is 2.5 m/s. The results show that CO_2 emission increases with pressure but attains a peak value of 2500 Pa. In the case of CO, the maximum emissions were about the same and do not vary significantly with fuel pressure. Figures 18 and 19 show the contours of CO2 and CO mole fractions for the port size of 1 mm, air velocity of 2.5 m/s, and fuel pressure of 2500 Pa, respectively. CO2 concentrations were highest in the fully reacted regions of the flame, indicating complete oxidation of carbon. Conversely, CO concentrations were highest in regions of incomplete combustion, particularly where oxygen was locally deficient.

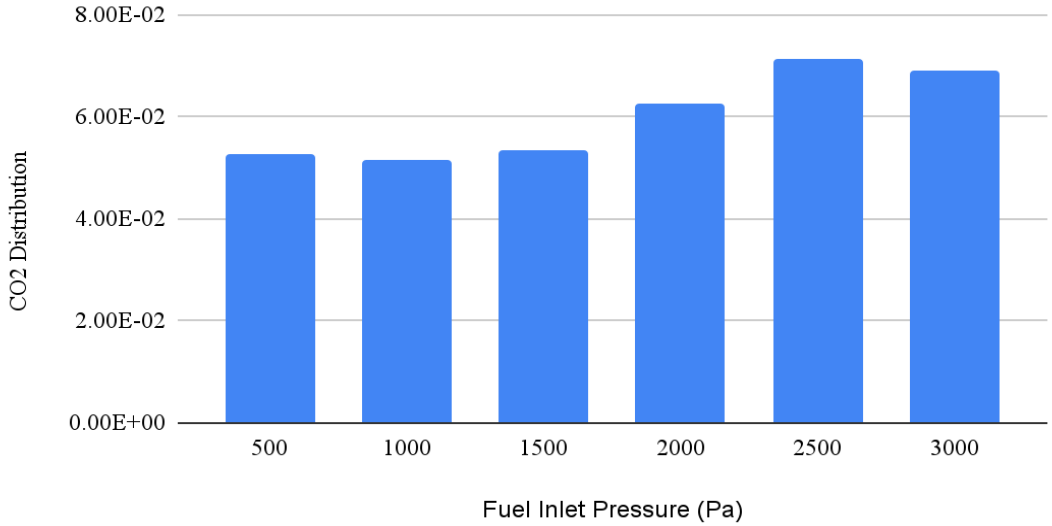

Figure 17: Graph of CO2 Distribution as the fuel inlet pressure is increased at a constant 2.5m/s air inlet velocity for a 1 mm burner port diameter

https://doi.org/10.70118/ujet.2026.sp01.15

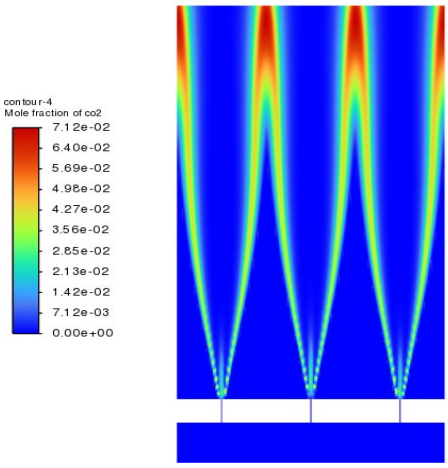

Figure 18: CO_2 distribution for 1 mm port diameter at 2500 Pa and 2.5 m/s air velocity

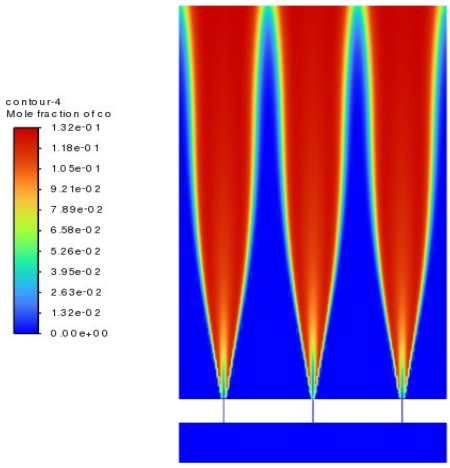

Figure 19: CO distribution for 1 mm port diameter at 2500 Pa and 2.5 m/s air velocity

Propane Distribution

The distribution of unburnt propane is inversely related to CO_2 and CO formation, showing high concentrations at the fuel inlet and rapid depletion within the domain. Figures 20 and 21 show the distribution of methane at fuel pressures of 500 and 3000 Pa, respectively, when the port size is 1 mm, and the air velocity is 2.5 m/s.

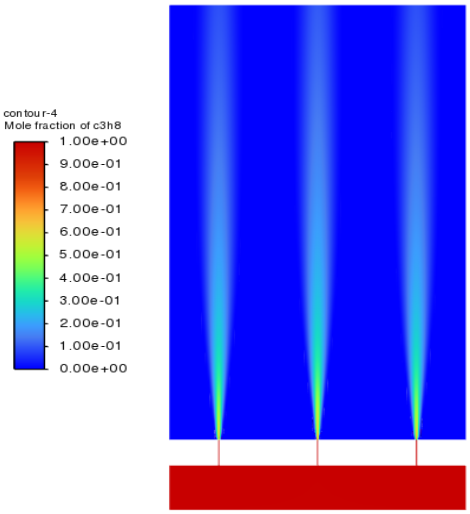

Figure 20: C_3H_8 distribution for 1 mm port diameter at 500 Pa and 2.5 m/s air velocity

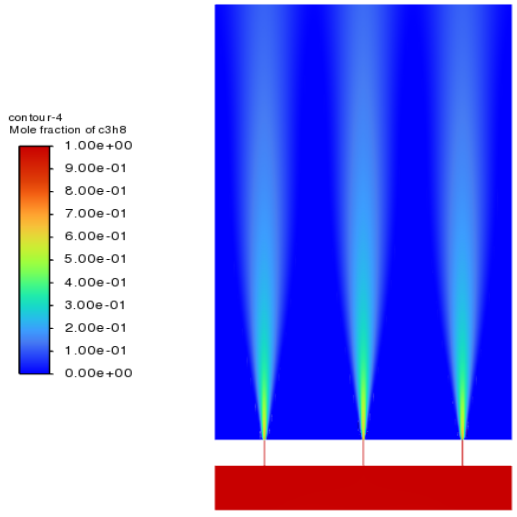

Figure 21: C_3H_8 distribution for 1 mm port diameter at 3000 Pa and 2.5 m/s air velocity

Soot Formation

The graph showing the relationship between fuel inlet pressure and soot formation is presented in Figure 22. Soot formation is distinctly low between 1500 and 2000 Pa, with a fuel pressure minimum at 2000 Pa. This pattern reflects the non-linear dependence of soot production on fuel injection pressure. Recent literature supports these observations. Edl et al. (2020) demonstrated that soot formation in propane combustion increases significantly when the oxygen concentration is elevated beyond 30%, primarily due to elevated temperatures and slower oxidiser mixing. Similarly, Kang et al. (2019) reported the correlation between higher pressure and high flame temperatures, which may explain the rise in soot concentration at 3000 Pa in this present study.

https://doi.org/10.70118/ujet.2026.sp01.15

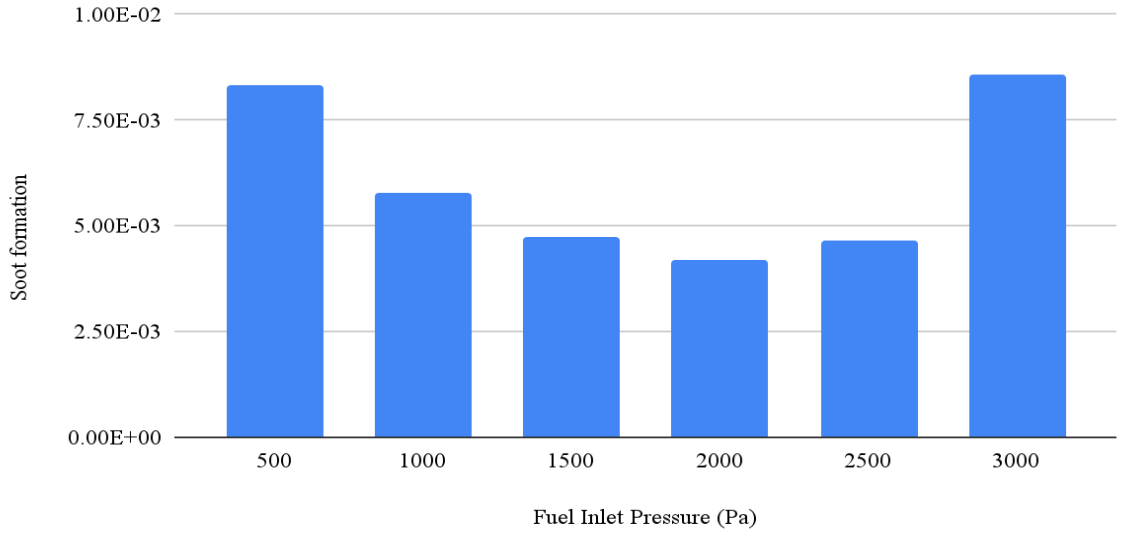

Figure 22: Pattern of soot formation as the fuel inlet pressure is increased at a constant 2.5m/s air inlet velocity for a 1 mm burner port diameter

NOx Formation

The graph shown in Figure 23 illustrates the influence of fuel inlet pressure on NO_x formation during propane combustion. The chart reveals a non-monotonic behaviour, with NO_x emissions initially decreasing between 500 Pa and 2000 Pa, followed by a rapid rise at higher pressures, particularly at 2500 Pa, peaking at 3000 Pa. These trends are well-supported by the work of Edl et al. (2018), where an increase in the concentration of oxygen in oxygen-enriched propane flames led to significant increases in NO_x formation due to higher peak flame temperatures. The study also demonstrated competitive interaction between soot and NO_x formation.

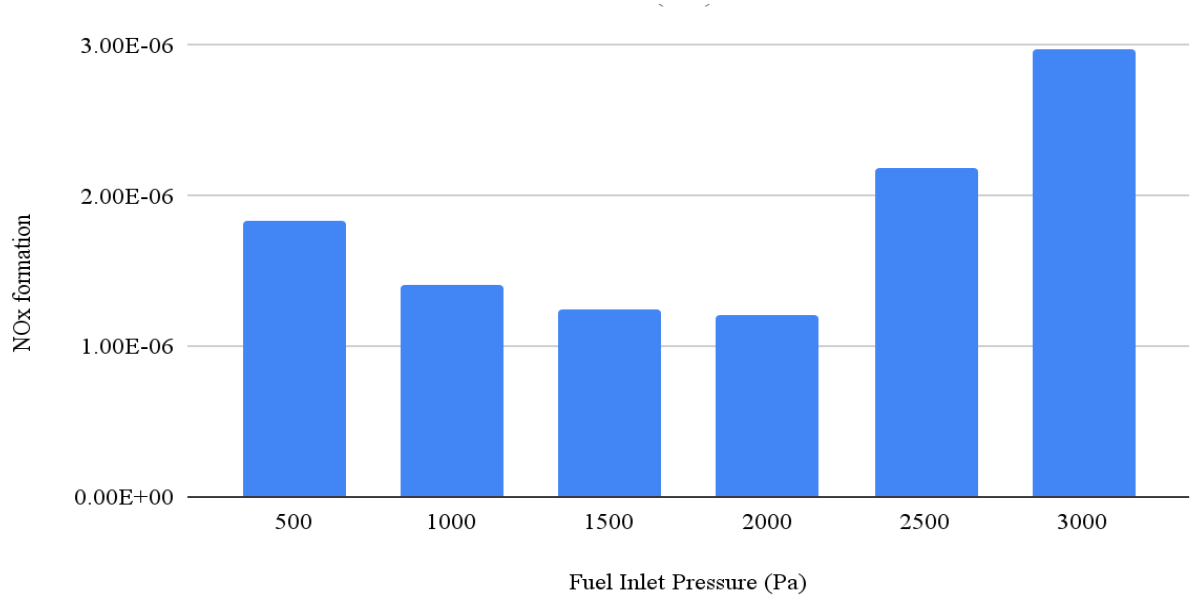

Figure 23: Pattern of NO_x formation as the fuel inlet pressure is increased at a constant 2.5m/s air inlet velocity for a 1 mm burner port diameter

Determination of Combustion Efficiency

The combustion efficiencies calculated for the 1 mm burner port diameter, 2.5 m/s air inlet velocity case, across varying fuel inlet pressures, are presented in Table 4.

https://doi.org/10.70118/ujet.2026.sp01.15

Table 4: Combustion Efficiency at Varying Fuel Inlet Pressures

Fuel Inlet Pressure	CO_2 mass fraction	CO mass fraction	Combustion Efficiency (%)
500	0.08227523	0.1336993	38.09
1000	0.08032761	0.1330119	37.65
1500	0.08348507	0.1325339	38.63
2000	0.09730867	0.13309	42.23
2500	0.1116622	0.1337466	45.50
3000	0.1080227	0.1360064	44.27

The results indicate that the highest combustion efficiency of 45.50% was achieved at a fuel inlet pressure of 2500 Pa and 2.5 m/s air inlet velocity, at a burner port diameter of 1 mm. Significantly, the highest peak flame temperature (2010 K) was observed under this specific condition. This indicates that, under this specific definition of combustion efficiency, the conditions leading to the most intense reaction also led to the most complete oxidation of carbon to CO_2 relative to CO. The efficiency shows a generally increasing trend with fuel pressure, peaking at 2500 Pa, before slightly decreasing at 3000 Pa, possibly due to excessive fuel flow.

These results align with ranges seen in conventional LPG burners without modifications. Pantangi et al. (2011) recorded a thermal efficiency of 68%, and Hussein et al. (2024) recorded that thermal efficiency increased from 30% to 52% with perforated plates. Khan et al. (2013) recorded thermal efficiencies of 48%, 50%, and 58% with different designs of burner heads.

4.0 Conclusion

This study has valuable insights into the operational characteristics and performance trade-offs of the cookstove. The key findings of this research include:

- The smallest burner port diameter (1 mm) and an optimal air inlet velocity (2.5 m/s) significantly improved fuel-air mixing due to increased jet momentum, leading to more concentrated reaction zones.
- The combination of a 1 mm port diameter, 2.5 m/s air inlet velocity, and 2500 Pa fuel inlet pressure yielded the highest peak flame temperature of about 2010 K.
- Higher fuel pressures (above 1500 Pa) led to increased CO and soot formation, indicating incomplete combustion. NO_x formation correlated directly with peak flame temperatures, with the 2500 Pa fuel pressure case showing the highest NO_x levels.
- The highest combustion efficiency of 45.50% was achieved at 2500 Pa fuel inlet pressure, which also corresponded to the highest peak temperature.
- Based on the findings of this research, the following recommendations can be made for designing and manufacturing burners for hybrid cookstoves in the near future:
- While 2500 Pa optimises carbon oxidation temperature, it also leads to higher NO_x and soot formation. Future design iterations should consider including secondary air injection components or modified burner geometries to further improve mixing and reduce these pollutants, even at high operating temperatures.
- The fuel used for cooking gas should be compared to a mixture of propane and butane to give a more realistic view of the liquified petroleum gas used for this purpose.
- The combustion kinetic mechanism may be extended to reduced or detailed mechanisms that will present the combustion of several species not accounted for by the 2-step chemistry used for this study.
- The study should be extended to a three-dimensional simulation to obtain more detailed results.

https://doi.org/10.70118/ujet.2026.sp01.15

References

Ali, H., & Wei, T. T. J. (2017). "CFD study of an improved biomass cookstove with reduced emissions and improved heat transfer characteristics". *Journal of Clean Energy Technologies*, 5(6), 427–432.

Bozzola, E., Agostiniani, R., Pacifici Noja, L., Park, J., Lauriola, P., Nicoletti, T., Taruscio, D., Taruscio, G., & Mantovani, A. (2024). "The impact of indoor air pollution on children's health and well-being: The experts' consensus". *Italian Journal of Paediatrics*, 50, Article 69.

Diti, P., & Šulc, R. (2024). "Calculations of CO_2 emission and combustion efficiency for various fuels". *Energy*, 290, Article 130044.

Dwivedi, G., Gohil, P. P., & Behura, A. K. (2021). "Numerical investigation of thermodynamic parameters for performance evaluation of cooking gas stove burner by appending of flame shield". *Materials Today: Proceedings*, 46, 5696–5702.

Edl, R., Allgurén, T., Normann, F., & Andersson, K. (2020). "Formation of soot in oxygen-enriched turbulent propane flames at the technical scale". *Energies*, 13(1), Article 191.

Fakinle, B. S., Oke, O. W., Odunlami, O. A., Sonibare, J. A., Akeredolu, F. A., & Oni, O. E. (2019). "Emission characterization and performance of conventional liquefied petroleum gas cookstove burners". *Cogent Engineering*, 6(1), Article 1652228.

Hamzah, D. A. (2015). "Theory comparison between propane and methane combustion inside the furnace". *International Journal of Current Engineering and Technology*, 5(4), 2429–2434.

Husain, Z., Tiwari, S. S., Pit, A. B., & Joshi, J. B. (2020). "Computational fluid dynamics study of biomass cook stove—Part 1: Hydrodynamics and homogeneous combustion". *Industrial & Engineering Chemistry Research*, 59(9), 4161–4176.

Kang, J., Ran, J., Niu, J., Shi, J., He, J., & Yang, Z. (2019). "Experimental and theoretical study on propane pyrolysis to produce gas and soot". *International Journal of Hydrogen Energy*, 44(39), 21762–21772.

Kuntikana, P., & Prabhu, S. V. (2019). "Thermal investigations on self-aspirating type radial flow burners with induced swirl". *Applied Thermal Engineering*, 161, Article 114118.

Magnussen, B. F., & Hjertager, B. H. (1977). "On mathematical modeling of turbulent combustion with special emphasis on soot formation and combustion". *Symposium (International) on Combustion*, 16(1), 719–729.

Matthujak, A., Wichangarm, M., Sriveerakul, T., Sucharitpwatskul, S., & Phongthanapanich, S. (2023). "Numerical and experimental study for a modified LPG cooking burner". *Journal of King Saud University – Science*, 35(6), Article 102752.

Pantangi, V. K., Mishra, S. C., Muthukumar, P., & Reddy, R. (2011). "Studies on porous radiant burners for LPG (liquefied petroleum gas) cooking applications". *Energy*, 36(10), 6074–6080.

Puzzolo, E., & Pope, D. (2017). "Clean fuels for cooking in developing countries". In *Encyclopedia of Sustainable Technologies* (pp. 289–297). Elsevier.

Rimar, M., Kizek, J., Kulikov, A., & Fedak, M. (2022). "Study of selected burner parameters on the gas-air mixture combustion". *MM Science Journal*, 2022(5), 6251–6256.

Rosenthal, J., Quinn, A., Grieshop, A. P., Pillarisetti, A., & Glass, R. I. (2018). "Clean cooking and the SDGs: Integrated analytical approaches to guide energy interventions for health and environment goals". *Energy for Sustainable Development*, 42, 152–159.

Schefer, R. W. (2001). "Reduced turbulence levels and combustion characteristics of a lifted propane jet flame". *Combustion and Flame*, 126(1–2), 1525–1535.

Setiawan, A. (2018). "Effective height of chimney for biomass cook stove simulated by computational fluid dynamics". *IOP Conference Series: Materials Science and Engineering*, 308(1), Article 012043.

Shahi, D. V. V., & Paraye, V. S. N. P. (2021). "Thermal analysis of domestic gas burner by design optimization of burner heads on CFD Fluent". *Materials Today: Proceedings*, 44(6), 3793–3799.

Sowgath, M. T., Rahman, M. M., Nomany, S. A., Sakib, M. N., & Junayed, M. (2015). "CFD study of biomass cooking stove using Autodesk simulation CFD to improve energy efficiency and emission characteristics". *Chemical Engineering Transactions*, 45, 1255–1260.

Turns, S. R. (2000). *An introduction to combustion: Concepts and applications* (2nd ed.). McGraw-Hill.

https://doi.org/10.70118/ujet.2026.sp01.15